IOP Publishing Nanotechnology
Nanotechnology 28 (2017) 415706 (8pp) https://doi.org/10.1088/1361-6528/aa825e

Few-layer MoS_2 as nitrogen protective barrier

B Akbali[1], A Yanilmaz[2], A Tomak[2], S Tongay[3], C Çelebi[1] and H Sahin[4,5,6]

[1] Department of Physics, Izmir Institute of Technology, 35430, Izmir, Turkey
[2] Department of Materials Science and Engineering, Izmir Institute of Technology, 35430, Izmir, Turkey
[3] School for Engineering of Matter, Transport and Energy, Arizona State University, Tempe, Arizona 85287, United States of America
[4] Department of Photonics, Izmir Institute of Technology, 35430, Izmir, Turkey
[5] ICTP-ECAR Eurasian Center for Advanced Research, Izmir Institute of Technology, 35430, Izmir, Turkey

E-mail: hasansahin@iyte.edu.tr

Received 12 May 2017, revised 23 July 2017
Accepted for publication 26 July 2017
Published 13 September 2017

Abstract

We report experimental and theoretical investigations of the observed barrier behavior of few-layer MoS_2 against nitrogenation. Owing to its low-strength shearing, low friction coefficient, and high lubricity, MoS_2 exhibits the demeanor of a natural N-resistant coating material. Raman spectroscopy is done to determine the coating capability of MoS_2 on graphene. Surface morphology of our MoS_2/graphene heterostructure is characterized by using optical microscopy, scanning electron microscopy, and atomic force microscopy. In addition, density functional theory-based calculations are performed to understand the energy barrier performance of MoS_2 against nitrogenation. The penetration of nitrogen atoms through a defect-free MoS_2 layer is prevented by a very high vertical diffusion barrier, indicating that MoS_2 can serve as a protective layer for the nitrogenation of graphene. Our experimental and theoretical results show that MoS_2 material can be used both as an efficient nanocoating material and as a nanoscale mask for selective nitrogenation of graphene layer.

Keywords: coating performance, MoS2, graphene, density functional theory, nitrogen doping, chemical vapor deposition, liquid exfoliation

(Some figures may appear in colour only in the online journal)

1. Introduction

Since its successful synthesis [1], graphene has become the most intensively studied form among the various carbon allotropes. Due to the strong sp^2 hybridization of carbon atoms and its single-atom thickness, graphene has exceptional properties such as advanced mechanical strength [2], high carrier mobility [3], and heat conduction [4] properties. These properties make graphene a rising star in the wide range of applications in nanodevices [5]. Following graphene, the interest in 2D transition-metal dichalcogenides such as MoS_2 has grown rapidly due to their superior properties such as unique quantum luminescence efficiency [6], high channel mobility($\sim$200 $cm^2\ V^{-1}\ s^{-1}$) [7], and large current ON/OFF ratio [8] (60 mV dec^{-1}) [9–16]. MoS_2 has indirect to direct gap transition from bulk to monolayer [17] and the presence of a band gap that does not exist in graphene makes it a suitable material for nanoscale electronic device applications.

It has been reported that different source/drain contacts determine the intrinsic transport properties of few-layer MoS_2 flakes [18]. Among exfoliation techniques [19, 20], liquid exfoliation is one of the promising method to obtain single-layer MoS_2 [21, 22]. Both its broad production methods and unique physical and chemical properties [6] make MoS_2 a promising material for various applications in electronics [23, 24], catalysis [25], chemical sensors [26], and lubrication [27], as well as for a protective layer to corrosion [28]. Bulk MoS_2 as a coating material has been investigated both

[6] Author to whom any correspondence should be addressed.

theoretically and experimentally for decades, because of its stable friction coefficient [29–31]. The anti-wear properties of MoS_2 have been examined theoretically [32] and experimentally [33] as an oxidation protective nanocoating material as well. In addition to MoS_2, other 2D materials such as WS_2 [32], graphene [34–38], and *h*-BN [28, 39–42] have been widely investigated both theoretically and experimentally as a protective layer against corrosion.

The incorporation of nitrogen (N) atoms into the crystal structure by N_2 plasma treatment is a practical method for modifying the physical and chemical properties of materials [43, 44]. With regard to graphene having semimetallic electronic structure, N is considered to be an excellent dopant, which is able to form strong covalent bonds by donating extra electrons into the graphene lattice [45, 46]. It has been reported that the incorporation of N in graphene may provide n- or p-type doping depending on the bonding character of the N atom [47, 48]. Such nitrogenated graphenes have been used in different applications such as lithium batteries [49, 50], bio-applications [51], field-effect transistors [52], supercapacitors [53], and oxygen reduction reaction in fuel cells [54–58]. Similarly, nitrogenation can also alter the electrical properties and chemical activity of MoS_2 crystal [59, 60]. McDonnell *et al* showed that MoS_2 can exhibit both p- and n-type at different positions on the same sample, which is attributed to variations in the local stoichiometry of MoS_2 due to surface defects [61]. In addition, Su *et al* showed that the increment of the number of N atoms causes an increase in the electron concentration, and therefore the Fermi level can be shifted towards the conduction band minimum [62].

In this study, we choose N_2 plasma treatment for the investigation of MoS_2 as a protective layer for graphene. Although the physical and chemical effects of N on MoS_2 have been examined [28, 63], the possibility of using MoS_2 as a protective coating material against nitrogenation for reactive surfaces such as graphene has not been reported yet. The paper is organized as follows. Detailed information about computational and experimental methodology are given in sections 2 and 3, respectively. First-principles calculation results are given in section 4. Finally, we discuss the results in section 5.

2. Computational methodology

For the investigation of the coating performance of MoS_2 against nitrogenation, we performed density functional theory (DFT)-based calculations implemented in the Vienna *ab initio* simulation package [64, 65]. The exchange-correlation energy was described by the generalized gradient approximation (GGA) using the Perdew–Burke–Ernzerhof functional [66]. The van der Waals (vdW) correction to the GGA functional was included by using the DFT-D2 method of Grimme [67].

The total energy difference between the sequential steps in the iterations was taken to be 10^{-5} eV for the convergence criterion. The total force in the unit cell was reduced to a value of less than 10^{-4} eV/Å. A plane-wave basis set with kinetic energy cutoff of 500 eV was used for all the calculations. To hinder interactions between the adjacent cells, at least 14 Å vacuum space was used along the *z*-direction. Spin-polarized calculations were performed in all cases. Analysis of the charge transfers in the structures was determined by the Bader technique [68].

The energetics of the vertical indentation and lateral diffusion of N are investigated by considering a 3×3 MoS_2 supercell. In the indentation calculations, the N atom approaches the MoS_2 layer in the appropriate path by fixing the vertical (all) coordinates at each step of 0.5 Å. In the lateral diffusion calculations, the lateral coordinates are fixed only on the chosen path. One of the Mo atoms, away from the indention and diffusion sites, is not allowed to relax and therefore fixes the vertical position of the MoS_2 layer in the supercell.

3. Experimental methodology

Graphene samples were grown on 25 μm thick Cu foil by the low pressure chemical vapor deposition (LPCVD) technique. Before the graphene growth, Cu samples were annealed for 80 min at 990 °C in a quartz chamber that was evacuated to a pressure of 10^{-5} Torr to increase the grain size on the Cu foil. The process was started at room temperature and throughout the process H_2 was utilized to reduce the native oxide layer on the Cu foil. The graphene growth reaction was carried out for 20 min at 850 °C, while introducing ethylene (C_2H_4), H_2, and Ar at a total pressure of about 1 Torr. All the samples were grown with C_2H_4, H_2, and Ar flow rates of 10, 30, and 150 sccm, respectively. The grown graphene films were transferred onto SiO_2 substrate. Graphene was transferred onto a desired substrate using the photoresist (PR) drop-casting method. Thick droplets of S1813 PR were drop-casted on graphene-holding Cu surfaces overnight in an oven at 70 °C to gently harden the PR. Then, the samples were immersed into $FeCl_3$ solution for etching the Cu foil. After the removal of the Cu foil, the graphene with PR layer was transferred onto DI water for 30 min to remove the $FeCl_3$ residue. Next, the sample was annealed at 70 °C for 30 s and 120 °C for 2 min to re-flow the PR on the graphene. This helped the PR to liquefy and release the graphene layers onto the target substrate. Removing the PR with acetone yielded a large area of graphene on the substrate.

MoS_2 samples were prepared by the liquid exfoliation method. Few-layer MoS_2 was prepared by mixing in 2–3 ml solutions of the MoS_2 powder dissolved in ethanol/water (0.5 mg/ml-2 mg/ml). The MoS_2 suspensions were sonicated for 120 min at a power of 225 W in a water-cooled bath. After the sonication, the final dispersions were centrifuged at 12000 rpm for 30 min and the top 3/4 of the supernatant was collected. The obtained MoS_2 samples were dissolved in ethanol/water, and dropped onto some part of the graphene/SiO_2 substrate.

The MoS_2/graphene samples were exposed to N_2 plasma in an RF-discharge plasma chamber. The chamber was pumped down to 30 mTorr and then filled with N_2 gas. After the pressure stabilization in the chamber at 30 mTorr, the capacity-coupled RF-discharge plasma was generated using an RF frequency generator. N_2 plasma treatment was applied

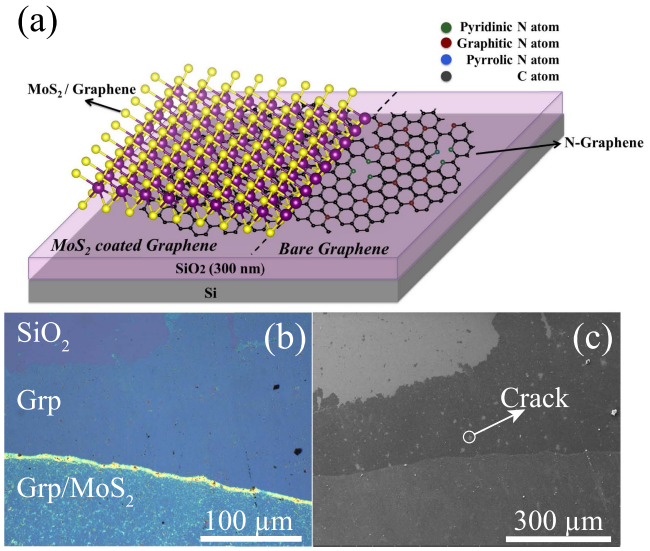

Figure 1. (a) Schematic illustration of MoS_2-coated and uncoated regions on the graphene layer. (b) OM and (c) SEM images of MoS_2-coated graphene.

using a high-purity N_2 gas with a flow rate of 40 sccm and RF forward power of 7 W. The chamber pressure was set to 1550 mTorr during the experiment. The duration of the nitrogenation was 15 min. After the nitrogenation process, the samples were first characterized by an optical microscope (OM) and scanning electron microscope (SEM), as shown in figure 1. Further analysis of the samples was done by Raman spectroscopy and atomic force microscopy (AFM) measurements.

4. Results and discussion

4.1. Adsorption, diffusion, and indentation of nitrogen atoms on MoS_2

In figure 1, we show OM and SEM images of MoS_2-coated graphene after nitrogenation. It can be clearly seen that while nitrogenation has a negligible effect on the structural properties of the MoS_2-coated region, the MoS_2-free graphene is significantly doped by nitrogen and therefore N-graphene domains are formed. Therefore, it appears that graphene and MoS_2 display quite different N-adsorption characteristics at the atomic level. In this section, to reveal how N atoms interact with MoS_2 layers, we perform state-of-the-art DFT calculations.

MoS_2 crystal is composed of vertically stacked layers interacting via vdW Force. Each single layer of MoS_2 consists of three sublayers in which a sublayer of Mo atoms is sandwiched between two sublayers of S atoms in a stacking order of ABA. This single-layer crystal structure of MoS_2 belongs to the $P\bar{6}m\bar{2}$ space group. Our total energy optimization calculations reveal that the lattice constant and Mo-S bond length are 3.19 and 2.41 Å, respectively. In addition, Bader charge analysis indicates that each Mo-S bond that has a

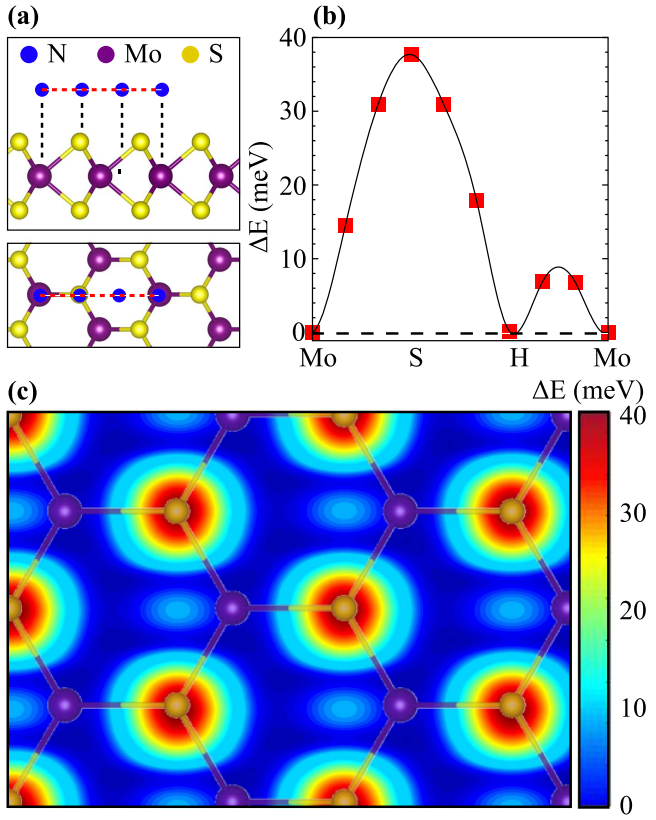

Figure 2. (a) Top and side views of the lateral diffusion path (dashed red line) of the N atom (blue circle) on MoS_2. Color code of the circles is given in the inset. (b) Energetics of nitrogen lateral diffusion. (c) 2D energy surface plot of the lateral diffusion of N.

covalent character is constructed through the contribution of 0.5 (1.0) electron from each S (Mo) atom.

As shown in figure 2(a), differing from graphene, diatomic MoS_2 crystal structure has three possible sites that provide favorable adsorption locations for N atoms: top hollow (H), top of molybdenum (Mo) atom, and top of sulfur (S) atom. Note that for adsorption calculations a 48-atom hexagonal supercell of MoS_2, which is enough large to hinder N-N interaction between the adjacent cells, is considered. We found that the N atom prefers to be located on top of the S atom with a bond length of 1.53 Å. Here, the binding energy is calculated to be 1.70 eV. The binding energy (E_b) of the N atom on MoS_2 is given by

$$E_b = E_{MoS_2} + E_N - E_{MoS_2+N}, \quad (1)$$

where E_{MoS_2}, E_N, E_{MoS_2+N} are the total optimized energy of the bare MoS_2, single nitrogen atom, and MoS_2-N system, respectively. Here, the S-N bond is formed through the 1.0e charge donation from N to the underlying S atom.

Then, we study lateral diffusion of the N atom through the most favorable adsorption sites. To simulate the N plasma treatment accurately, the initial position of the N atom is fixed at in-plane directions and allowed to relax in the perpendicular direction. As shown in figure 2(b), Mo and H sites are most favorable diffusion sites. However, for diffusion from Mo to H sites through the S atom, the energy barrier is calculated to be 38 meV. Considering the position-dependent

energy curve around the Mo site as a harmonic potential, the jump frequency of the N atom is calculated to be $\nu \approx 36$ THz. Obviously, the high jump frequency arises from the low lateral diffusion barrier (38 meV). In addition, there is another local diffusion barrier of 8 meV between the Mo and H sites (see figure 2(b)).

Moreover, we present a 2D energy landscape of the adsorption sites in figure 2(c). It appears that the N atom is able to diffuse on the MoS_2 layer by following the path that connects the Mo and H sites through the line between the S atoms. Considering our experiment for the plasma treatment, one may expect adsorption on N atoms on S sites and also their lateral diffusion on MoS_2 surfaces.

In addition, vertical diffusion of N atoms through the MoS_2 layers may also take place during the nitrogen plasma treatment. At the atomic level, depending on the kinetic energy of the approaching N atoms, such a vertical diffusion can happen in two different ways: (i) N atoms diffuse via a strong interaction with neighboring Mo and S atoms or (ii) N atoms rapidly diffuse through the hollow site by weak interaction with neighboring atoms.

As shown in figure 3(a), approaching N atom starts to see the local potential of the MoS_2 layer from a distance of 5 Å and finds a local energy minimum 2.5 Å over the surface (**I** point). At such local minima, N atoms are simply physisorbed with a binding energy of 100 meV. However, to reach the global minimum at point **III**, where the chemical adsorption takes place, N atoms can easily overcome the energy barrier at point **II**. It can also be seen that once N atoms are chemisorbed, there is a huge energy barrier (2.2 eV) for further indentation towards the MoS_2 layer.

As the second scenario for vertical diffusion, figure 3(b) shows that when N atoms pass through hollow sites without forming bonds with neighboring Mo and S atoms they experience much larger energy barriers. For instance, the energy barrier to reach the S level (at point **II**) is calculated to be 1.5 eV. We can also see that N atoms can find a local minimum at the Mo level (at point **III**) once they are able pass through the S level. Then, N atoms see another large energy barrier when going from the Mo level to the lowermost S level (at point **IV**).

To sum up, we investigated the interaction of N atoms with MoS_2 crystal structure by calculating (i) geometry optimization calculations for N atoms on MoS_2 layer, (ii) possible lateral diffusion paths and required energy barriers and, (iii) two different vertical diffusion mechanisms. Our results clearly show that N atoms can be adsorbed on the MoS_2 surface and due to the small energy barriers they are also able to diffuse laterally. However, their vertical penetration inside the layers is not likely to occur during the plasma treatment.

4.2. Raman spectroscopy results

Raman spectroscopy measurements were carried out to observe the structural properties of MoS_2/graphene heterostructure against nitrogenation. Figure 4 shows the Raman spectra of MoS_2/graphene on SiO_2/Si substrate before and after the plasma treatment. It should be noted that the Raman spectrum of MoS_2/graphene films was taken from the same region before and after the nitrogenation process.

Raman signals were recorded in a spectral range between 225–490 and 1200–3500 cm^{-1} using an Ar^+ ion laser with 532 nm excitation (1800 grooves/mm grating) wavelength to observe all the characteristic peaks of MoS_2 and graphene before and after the nitrogenation process. For each sample, the Raman experiment was repeated five times to check the reproducibility of the measurement. Each spectrum was normalized using LabSpec software.

Since the main Si and SiO_2 peaks seen at 521 and 900–1000 cm^{-1}, repressed the characteristic peaks of graphene and MoS_2, they were extracted from the total Raman spectra. After the extraction process, the peaks of graphene and MoS_2 became dominant and another weak feature around 300 cm^{-1} became visible. This peak corresponds to the SiO_2 on the silicon substrate [69].

Two preponderant Raman active modes of ultra-thin MoS_2 are measured at 381 cm^{-1} (E′), and 403 cm^{-1} (A_1) (see figure 4). The E′ mode arises from the opposite vibration of two S atoms against the Mo atom, while A_1 mode has an out-of-plane characteristic, which corresponds to the vibration of only S atoms in the opposite direction [70]. Li *et al* reported that the frequency difference between E′ and A_1 decreases when the thickness of the MoS_2 diminishes [71]. This behavior occurred through the reduction of the long-range Coulomb interaction, which originates from the increment of the dielectric constant of the material [70]. In addition, we measured a mode centered at 227 cm^{-1}, which corresponds to the longitudinal acoustic mode [71, 72].

The D, G, and G′ peaks are the predominant features in the spectrum of N-graphene as in pristine graphene. When defects or damages occur in the graphene flake, D, D′, and their combination (D+D′) peaks appear in the Raman spectrum of graphene [73]. They are characterized by the peaks at around 1350, 1585, and 2680 cm^{-1}, respectively. The D′ and D+D′ peaks appear at 1625 and 2940 cm^{-1}, respectively. The G band corresponds to the doubly-degenerate E_{2g} phonons at the Brillouin zone. The G′ and D bands are all induced by the second-order, double-resonance process and are related to zone-boundary phonons. The scattering process involves two zone-boundary phonons for G′ mode; it involves one phonon and one defect for the D mode. While the D band requires defects to activate it, the G′ band does not require the activation of the defects. Thus, the G′ band is always seen in the Raman spectra of graphene and N-graphene, even when the D band is not observed. In addition, the D′ band arises from the intra-valley, defect-induced, double-resonance process [54, 74]. Another peak, which is the D+D′ band is the combination of phonons with different momenta around K and Γ, thus requiring a defect for its activation [75, 76].

As can be seen in figure 4, the two intense peaks, G peak at ∼1590 cm^{-1} and G′ peak at ∼2700 cm^{-1}, can be clearly observed for graphene. The peak at ∼1350 cm^{-1}, D peak was presumed to be related to the domain boundaries and growth nucleation sites, and its intensity increased after the nitrogenation process with respect to that of pristine graphene. The

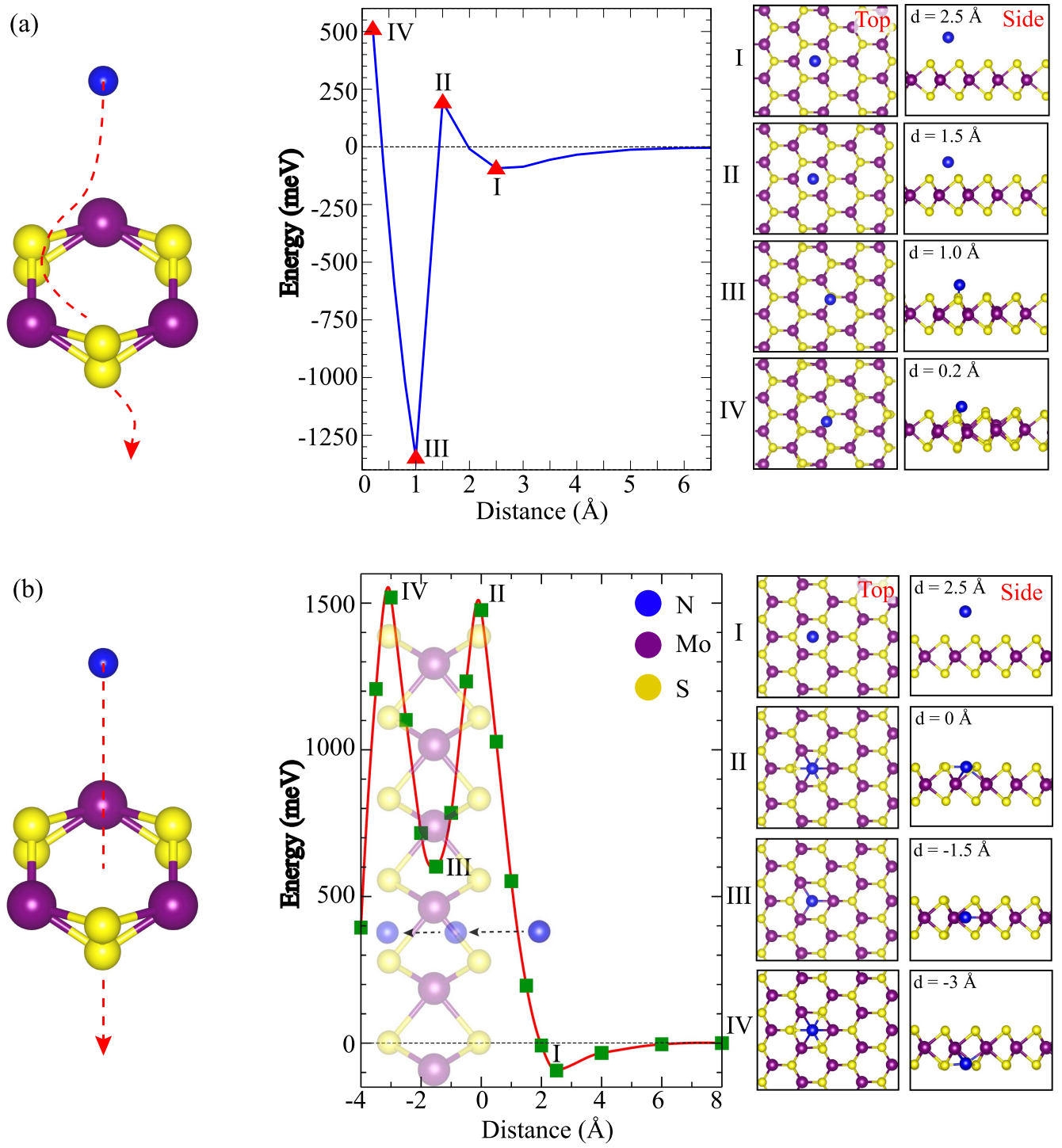

Figure 3. Variation of the relative energy of the MoS_2+N system (a) when the N is free to move in the plane direction and (b) when it is fixed at each step. In (a), S-N bond occurrence results in minimum energy at 1 Å. In (b), N is forced to pass through the hollow site. Here, D stands for vertical distance between the N atom and upper S atom.

D′ peak (~1630 cm^{-1}) in the Raman spectrum of N-graphene that was attributed to the inter-valley double-resonance scattering process, emerged after the plasma process [73, 77]. In addition, a faint peak at ~2940 cm^{-1}, the D+D′ peak is also observed due to the sign of the atomic insertions in the spectral region [78, 79]. These results show that the nitrogenation process leads to the appearance of a strong D peak, as well as the emergence of the D′ and D+D′ peaks. This also suggests that the graphene lattice becomes somewhat disordered after the nitrogenation process.

4.3. AFM results

We also investigated the morphology of graphene and MoS_2/graphene structures by tapping mode AFM (figure 5) measurements under ambient conditions. All the measurements

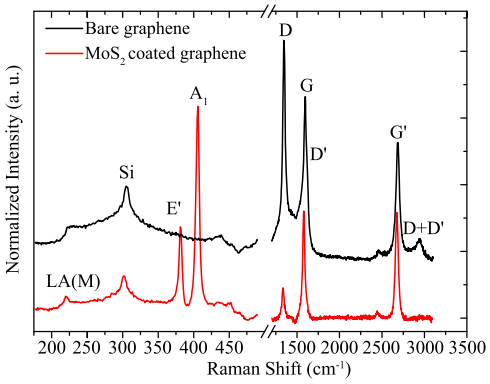

Figure 4. Raman measurement of graphene and MoS_2/graphene regions after nitrogenation process. The main Si and SiO_2 peaks located at at the spectral region between 450 and 1250 cm^{-1} were extracted from the total spectra. Nitrogenation parameters: nitrogen gas flow 40 sccm, effective RF power 7 W, plasma time 15 min, nitrogen pressure 1550 mTorr.

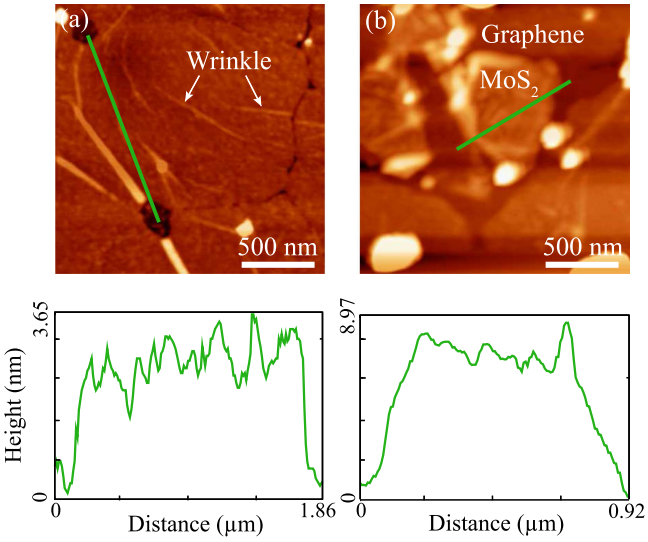

Figure 5. Tapping mode AFM images of graphene (a) and MoS_2/graphene (b) on SiO_2/Si substrate with corresponding line profiles.

were conducted with 512 × 512 data acquisitions at various scan speeds. Oxide-sharpened silicon nitride tips with an integrated cantilever (with a nominal spring constant of 48 N/m) were used. For AFM topography measurements, a drop of the MoS_2 suspension was fixed on the graphene coated SiO_2/ Si substrate. The AFM images and corresponding line profiles of graphene grains on SiO_2/Si substrate can be seen in figures 5(a) and (c), respectively.

Some wrinkles, which are indicated by the arrows, were observed due to the thermal expansion coefficient mismatch between the Cu surface and graphene film during the cooling process (figure 5(a)) [80]. Moreover, small bright particles, related to SiO_2 traces were observed in the AFM image, as reported in similar works [81, 82]. Si-enriched SiO_2 particles arise from the quartz tube used in the CVD chamber. Since the Si particles from the quartz tube react with oxygen (found in Cu foil surface) at high temperatures under LPCVD condition, the formation of SiO_2 can be observed on the surface of the sample after the graphene growth procedure. Therefore, they are more likely to be transferred together with graphene onto the SiO_2/Si. The height of the graphene on the SiO_2/Si substrate was determined to be 3.7 nm (see figure 5(c)). This thickness corresponds to few-layer graphene [83] and this obtained result is in good agreement with the Raman spectroscopy result of the pristine graphene. We found that the graphene grain size ranged between 2–4 nm (see figure 5).

We analyzed the MoS_2 nanoflakes after they were dropped onto the graphene layer. A high-resolution AFM image of the MoS_2/graphene heterostructure on the SiO_2/Si substrate is shown in figure 5(b). It can be clearly seen that the height of the heterostructure is 9–10 nm as measured by the line profile acquired from the AFM image (see figure 5(d)). An average thickness of the MoS_2 flakes was found to be 5 nm. The MoS_2 flake size ranged between 2 and 4 nm, as determined by AFM (see figure 5(b)).

5. Conclusion

In this study, we have investigated the coating performance of MoS_2 against nitrogenation both experimentally and theoretically. The present work shows the effect of the 2D stacking of MoS_2 and graphene vdW layers on their behavior under nitrogen plasma treatment. Raman spectroscopy analysis revealed that the nitrogenation process leads to the appearance of a strong D peak, as well as the emergence of a D′ and D+D′ peak on bare graphene. However, these findings were not observed on the few-layer MoS_2-coated graphene region. Experimental results were also consistent with first-principles calculations. Our calculations exhibited that (1) N atom diffuses in a lateral direction by following the path through the molybdenum (Mo) and hollow (H) sites, (2) MoS_2 shows high energy barrier against penetration of the nitrogen atom, and (3) large-area defect-free MoS_2 can serve as an ideal nanocoating material, which can protect the underlying surface from nitrogenation. To sum up, the MoS_2 material can be used either as an effective nanocoating material or as a nanoscale mask for the selective nitrogenation of graphene.

Acknowledgments

Computational resources were provided by TUBITAK ULAKBIM, High Performance and Grid Computing Center (TR-Grid e-Infrastructure). HS acknowledges financial support from the TUBITAK under project number 116C073. HS acknowledges support from Bilim Akademisi-The Science Academy, Turkey, under the BAGEP program. This project was partly supported by the National Science Foundation USA (NSF DMR-1552220). The authors thank Dilce Özkendir and Cihan Bacaksiz for their fruitful discussions.

References

[1] Novoselov K S, Geim A K, Morosov S V, Jiang D, Katsnelson M I, Grigorieva I V, Dubonos S V and Firsov A A 2004 *Science* **306** 666
[2] Ovid'ko I A 2013 *Rev. Adv. Mater. Sci.* **34** 1
[3] Neto A C, Guinea F, Peres N M, Novoselov K S and Geim A K 2009 *Rev. Mod. Phys.* **81** 109
[4] Balandin A A, Ghosh S, Bao W, Calizo I, Teweldebrhan D, Miao F and Lau C N 2008 *Nano Lett.* **8** 902
[5] Vicarelli L, Vitiello M S, Coquillat D, Lombardo A, Ferrari A C, Knap W, Polini M, Pellegrini V and Tredicucci A 2012 *Nat. Mater.* **11** 865
[6] Mak K F, Lee C, Hone J, Shan J and Heinz T F 2010 *Phys. Rev. Lett.* **105** 136805
[7] Radisavljevic B, Radenovic A, Brivio J, Giacometti V and Kis A 2011 *Nat. Nano* **6** 147
[8] Yoon Y, Ganapathi K and Salahuddin S 2011 *Nano Lett.* **1** 3768
[9] Kong D, Wang H, Cha J J, Pasta M, Koski K J, Yao J and Cui Y 2013 *Nano Lett.* **13** 1341
[10] Zhang Y *et al* 2014 *Nat. Nano* **9** 111
[11] Fang H, Chuang S, Chang T C, Takei K, Takahashi T and Javey A 2012 *Nano Lett.* **12** 3788
[12] Ali M N, Xiong J, Flynn S, Tao J, Gibson Q D, Schoop L M, Liang T, Haldolaarachchige N, Hirschberger M, Ong N P and Cava R 2015 *Nature* **514** 2015
[13] Keum D H *et al* 2015 *Nature Phys.* **11** 482
[14] Ramakrishna Matte H S S, Gomathi A, Manna A K, Late D J, Datta R, Pati S K and Rao C N R 2010 *Angew. Chem.* **122** 4153
[15] Georgiou T *et al* 2013 *Nat. Nano* **8** 100
[16] Splendiani A, Sun L, Zhang Y, Li T, Kim J, Chim C-Y, Galli G and Wang F 2010 *Nano Lett.* **10** 1271
[17] Wang Q H, Kalantar-Zadeh K, Kis A, Coleman J N and Strano M S 2012 *Nat. Nano* **7** 699
[18] Das S, Chen H-Y, Penumatcha A V and Appenzeller J 2013 *Nano Lett.* **13** 100
[19] Eda G, Yamaguchi H, Voiry D, Fujita T, Chen M and Chhowalla M 2011 *Nano Let.* **11** 5111
[20] Xiao J, Choi D, Cosimbescu L, Koech P, Liu J and Lemmon J P 2010 *Chem. Mater.* **22** 4522
[21] Coleman J N *et al* 2011 *Science* **331** 658
[22] Lee K, Kim H-Y, Lotya M, Coleman J N, Kim G-T and Duesberg G S 2011 *Adv. Mater.* **23** 4178
[23] Wu W *et al* 2014 *Nature* **514** 470
[24] Li H, Yin Z, He Q, Li H, Huang X, Lu G, Fam D W H, Tok A I Y, Zhang Q and Zhang H 2012 *Small* **8** 63
[25] Miremadi B K and Morrison S R 1987 *J. Catal.* **103** 334
[26] Zhang H, Loh K P, Sow C H, Gu H, Su X, Huang C and Chen Z K 2004 *Langmuir* **20** 6914
[27] Rapoport L, Bilik Yu, Feldman Y, Homyonfer M, Cohen S R and Tenne R 1997 *Nature* **387** 791
[28] Vandana S *et al* 2017 *J. Phys. D: Appl. Phys.* **50** 045301
[29] Donnet C, Martin J M, Le Mogne Th and Belin M 1996 *Tribol. Int.* **29** 112
[30] Martin J M, Donnet C, Mogne T L and Epicier T 1993 *Phys. Rev.* B **48** 10583
[31] Wahl K J, Belin M and Singer I L 1998 *Wear* **214** 212
[32] Sen H S, Sahin H, Peeters F M and Durgun E 2014 *J. Appl. Phys.* **116** 083508
[33] Park W, Park J, Jang J, Lee H, Jeong H, Cho K, Hong S and Lee T 2013 *Nanotechnology* **24** 095202
[34] Raman R K S, Banerjee P C, Lobo D E, Gullapalli H, Sumandasa M, Kumar A, Choudhary L, Tkacz R, Ajayan P M and Majumder M 2012 *Carbon* **50** 4040
[35] Topsakal M, Şahin H and Ciraci S 2012 *Phys. Rev.* B **85** 155445
[36] Schriver M, Regan W, Gannett W J, Zaniewski A M, Crommie M F and Zettl A 2013 *ACS Nano* **7** 5763
[37] Chen S *et al* 2011 *ACS Nano* **5** 1321
[38] Kirkland N, Schiller T, Medhekar N and Birbilis N 2012 *Corros. Sci.* **56** 1
[39] Liu Z, Gong Y, Zhou W, Ma L, Yu J, Idrobo J C, Jung J, MacDonald A H, Vajtai R, Lou J and Ajayan P M 2013 *Nat. Commun.* **4** 2541
[40] Li L H, Xing T, Chen Y and Jones R 2014 *Adv. Mater. Interfaces* **1** 1300132
[41] Shen L, Zhao Y, Wang Y, Song R, Yao Q, Chen S and Chai Y 2016 *J. Mater. Chem.* A **4** 5044
[42] Li L H, Cervenka J, Watanabe K, Taniguchi T and Chen Y 2014 *ACS Nano* **8** 1457
[43] Talbi A, Benamara Z, Akkal B, Gruzza B, Bideux L, Robert C, Varenne C and Chami N 2006 *Mater. Sci. Eng.* A **437** 254
[44] Patel P, Nadesalingam M, Wallace R M and Buchanan D A 2009 *J. Appl. Phys.* **105** 024517
[45] Akada K, Tomo-o Terasawa, Imamura G, Obata S and Saikia K 2014 *Appl. Phys. Lett.* **104** 131602
[46] Rybin M, Pereyaslavtsev A, Vasilieva T, Myasnikov V, Sokolov I, Pavlova A, Obraztsova E, Khomich A, Ralchenko V and Obraztsova E 2016 *Carbon* **96** 196
[47] Lu Y-F, Lo S-T, Lin J-C, Zhang W, Lu J-Y, Liu F-H, Tseng C-M, Lee Y-H, Liang C-T and Li L-J 2013 *ACS Nano* **7** 6522
[48] Wu T, Shen H, Sun L, Cheng B, Liu B and Shen J 2012 *New J. Chem.* **36** 1385
[49] Reddy A L M, Srivastava A, Gowda S R, Gullapalli H, Dubey M and Ajayan P M 2010 *ACS Nano* **4** 6337
[50] Wang H, Zhang C, Liu Z, Wang L, Han P, Xu H, Zhang K, Dong S, Yao J and Cui G 2011 *J. Mater. Chem.* **21** 5430
[51] Wang Y, Shao Y, Matson D W, Li J and Lin Y 2010 *ACS Nano* **4** 1790
[52] Zhang C, Fu L, Liu N, Liu M, Wang Y and Liu Z 2011 *Adv. Mater.* **23** 1020
[53] Jeong H M, Lee J W, Shin W H, Choi Y J, Shin H J, Kang J K and Choi J W 2011 *Nano Lett.* **11** 2472
[54] Bao J F, Kishi N and Soga T 2014 *Mater. Lett.* **117** 199
[55] Wang H, Maiyalagan T and Wang X 2012 *ACS Catal.* **2** 781
[56] Park S H, Chae J, Cho M-H, Kim J H, Yoo K-H, Cho S W, Kim T G and Kim J W 2014 *J. Mater. Chem.* C **2** 933
[57] Qu L, Liu Y, Baek J-B and Dai L 2010 *ACS Nano* **4** 1321
[58] Jafri R I, Rajalakshmi N and Ramaprabhu S 2010 *J. Mater. Chem.* C **20** 7114
[59] Qin S, Lei W, Liu D and Chen Y 2014 *Sci. Rep.* **4** 7582
[60] Liu Q, Weijun X, Wu Z, Huo J, Liu D, Wang Q and Wang S 2016 *Nanotechnology* **27** 175402
[61] McDonnell S, Addou R, Buie C, Wallace R M and Hinkle C L 2014 *ACS Nano* **8** 2880
[62] Su T-H and Lin Y-J 2016 *Appl. Phys. Lett.* **108** 033103
[63] Azcatl A *et al* 2016 *Nano Lett.* **16** 5437
[64] Kresse G and Hafner J 1993 *Phys. Rev.* B **47** 558
[65] Kresse G and Furthmuller J 1996 *Phys. Rev.* B **54** 11169
[66] Perdew J P, Burke K and Ernzerhof M 1996 *Phys. Rev. Lett.* **77** 3865
[67] Grimme S 2006 *J. Comput. Chem.* **27** 1787
[68] Henkelman G, Arnaldsson A and Jonsson H 2006 *Comput. Mater. Sci.* **36** 354
[69] Balendhran S, Ou J Z, Bhaskaran M, Sriram S, Ippolito S, Vasic Z, Kats E, Bhargava S, Zhuiykov S and Kalantar-Zadeh K 2012 *Nanoscale* **4** 461
[70] Molina-Sanchez A and Wirtz L 2011 *Phys. Rev.* B **84** 155413
[71] Li H, Zhang Q, Ray Yap C-C, Tay B K, Tong Edwin T-H, Olivier A and Baillargeat D 2012 *Adv. Funct. Mater.* **22** 1385
[72] Frey G L, Tenne R, Matthews M J, Dresselhaus M S and Dresselhaus G 1999 *Phys. Rev.* B **60** 2883
[73] Beams R, Cançado L G and Novotny L 2015 *J. Phys. Condens. Matter* **27** 083002

[74] Pimenta M, Dresselhaus G, Dresselhaus M S, Cancado L, Jorio A and Saito R 2007 *Phys. Chem. Chem. Phys.* **9** 1276
[75] Iqbal M, Singh A K, Iqbal M and Eom J 2012 *J. Phys. Condens. Matter* **24** 335301
[76] Wang C, Zhou Y, He L, Ng T-W, Hong G, Wu Q-H, Gao F, Lee C-S and Zhang W 2013 *Nanoscale* **5** 600
[77] Zafar Z, Ni Z H, Wu X, Shi Z X, Nan H Y, Bai J and Sun L T 2013 *Carbon* **60** 57
[78] Ye D, Wu S-Q, Yu Y, Liu L, Lu X-P and Wu Y 2014 *Appl. Phys. Lett.* **104** 103105
[79] Majumdar A, Schäfer J, Mishra P, Ghose D, Meichsner J and Hippler R 2007 *Surf. Coat. Technol.* **201** 6437
[80] Meng L, Su Y, Geng D, Yu G, Liu Y, Dou R-F, Nie J-C and He L 2013 *Appl. Phys. Lett.* **103** 251610
[81] Jung D H, Kang C, Kim M, Cheong H, Lee H and Lee J S 2014 *J. Phys. Chem.* C **118** 3574
[82] Hedayat S M, Karimi-Sabet J and Shariaty-Niassar M 2017 *Appl. Surf. Sci.* **399** 542
[83] Shearer C J, Slattery A D, Stapleton A J, Shapter J G and Gibson C T 2016 *Nanotechnology* **27** 125704